Vibration analysis and control of the LIGO observatories large chambers and support piers

Conference Paper · September 2014

7 authors, including:

David Tshilumba
GDF SUEZ
8 PUBLICATIONS   **34** CITATIONS

SEE PROFILE

Fabrice Matichard
Massachusetts Institute of Technology
225 PUBLICATIONS   **27,258** CITATIONS

SEE PROFILE

C. Collette
Université Libre de Bruxelles
207 PUBLICATIONS   **48,872** CITATIONS

SEE PROFILE

Some of the authors of this publication are also working on these related projects:

CLIC Project View project

TALC - The Thinned Aperture Light Collector View project

Vibration analysis and control of the LIGO observatories large chambers and support piers

D. Tshilumba[1], L. K. Nuttall[2], T. Mac Donald[3], R. Mittleman[4], B. Lantz[3], F. Matichard[4,5], C. Collette[1]

[1] Université Libre de Bruxelles, BEAMS department,
50 F.D. Roosevelt av., 1050 Brussels (Belgium)
e-mail: **ccollett@ulb.ac.be**

[2] Center for gravitation and cosmology, University of Wisconsin–Milwaukee,
Milwaukee, WI 53211, USA

[3] Stanford University, Ginzton Laboratory,
Stanford, CA. 94305-4088(United States)

[4] Massachusetts Institute of Technology,
185 Albany St., NW22-295 Cambridge, MA. 02139 (US)

[5] California Institute of Technology,
1200 East California Boulevard, Pasadena California 91125 (US)

Abstract

The Laser Interferometer Gravitational wave Observatories (LIGO) host kilometers long vacuum equipment. At each site, five large chambers and support structures are used to store the detector's core instrumentation. This article discusses the vibrations of these large vacuum chambers and equipment. It presents and summarizes transmissibility measurements performed at the LIGO test facilities and observatories. In addition, it presents detailed models and compares them with experiments and discusses vibration mitigation techniques and control options. It concludes with recommendations for future LIGO observatories.

1   Introduction

Several scientific instruments dedicated to experimental physics are made of very sensitive equipment mounted on large structures. For example: space telescopes mounted on large truss structures [1], electromagnets of particle colliders mounted on large superstructures [2], mirrors of gravitational wave detectors mounted on high pier structures [3]. Even though the precision required in the aforementioned examples may differ by several orders of magnitues, the quality of the observation is always compromised by the vibrations of the supporting structure. In this paper, we study an example of large and heavy structures: the support piers and vaccum chambers located in the LIGO gravitational wave detectors.

The LIGO Observatories use 4 km long interferometers designed to detect gravity waves produced by astrophysical events [4]. The two LIGO sites are located in the US, in Livingston LA, and Hanford WA. The construction of a third observatory in India is currently being studied. The interferometer operates in an ultra-high-vacuum system. Five large vacuum chambers host the core optics of the detectors. A Computer Aided Drawing representation (CAD) of the LIGO vacuum system and large vacuum chambers is shown in Figure 1. For each chamber, the isolated optics is supported by huge blue piers.

The paper is laid out as follows. Section two of this paper shows transmissibility measurements performed at the LIGO test facilities (LASTI) and observatories to highlight the motion amplification induced by the vibration of the large chamber and supporting structure. Section three focuses on the modeling of the system and section four discusses mitigation and control options. The last section presents conclusions.
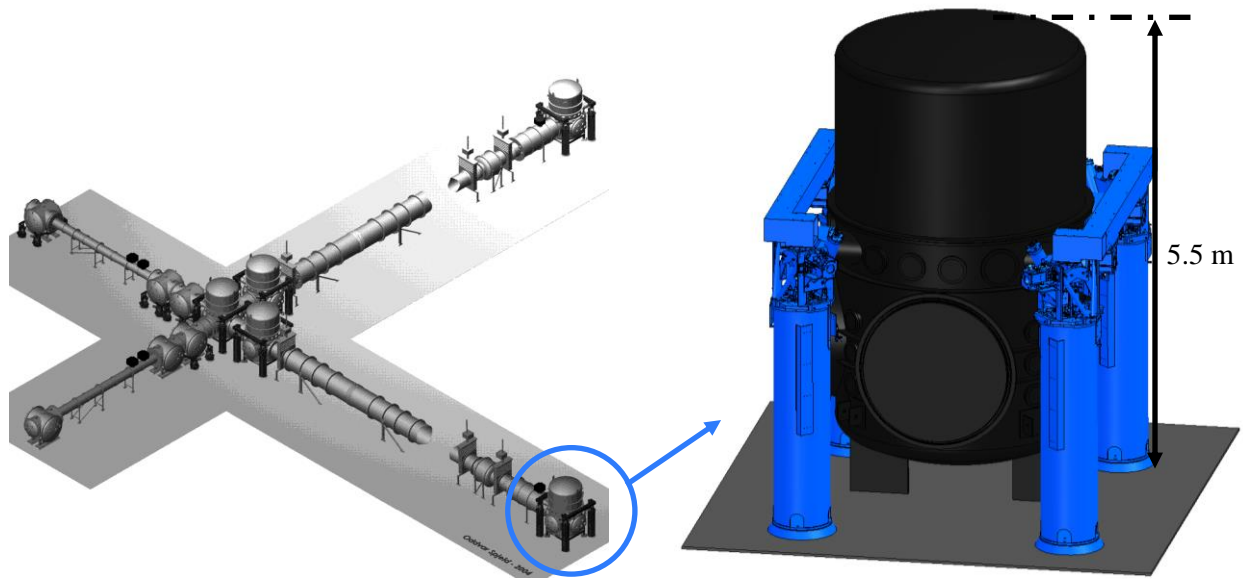
Figure 1: (a) CAD representation of the the LIGO vaccum Sytem. (b) One of the five LIGO large vaccum chambers equipment used at each site.

2   Transmissibility measurements

2.1   LASTI

The LIGO test facility at MIT (Cambridge MA), also known as LASTI, houses chambers and support piers which are identical to those used at the LIGO sites. The ground and concrete characteristics differ between LASTI and the sites; nevertheless this equipment is a good bench to analyze the vibrations of this system. Figure 2a shows an image of the large chamber equipment at the LIGO test facility. Figure 2b shows an example of the transmissibility between the ground and the top of the piers (shown in Figure 2a). The ground motion is amplified by as much as a factor of 25 at the first resonance peak at 10 Hz. The amplitude of the second resonance peak is near a factor of 20. The model fit shows that the transmissibility falls as the forth power of frequency after the second mode.
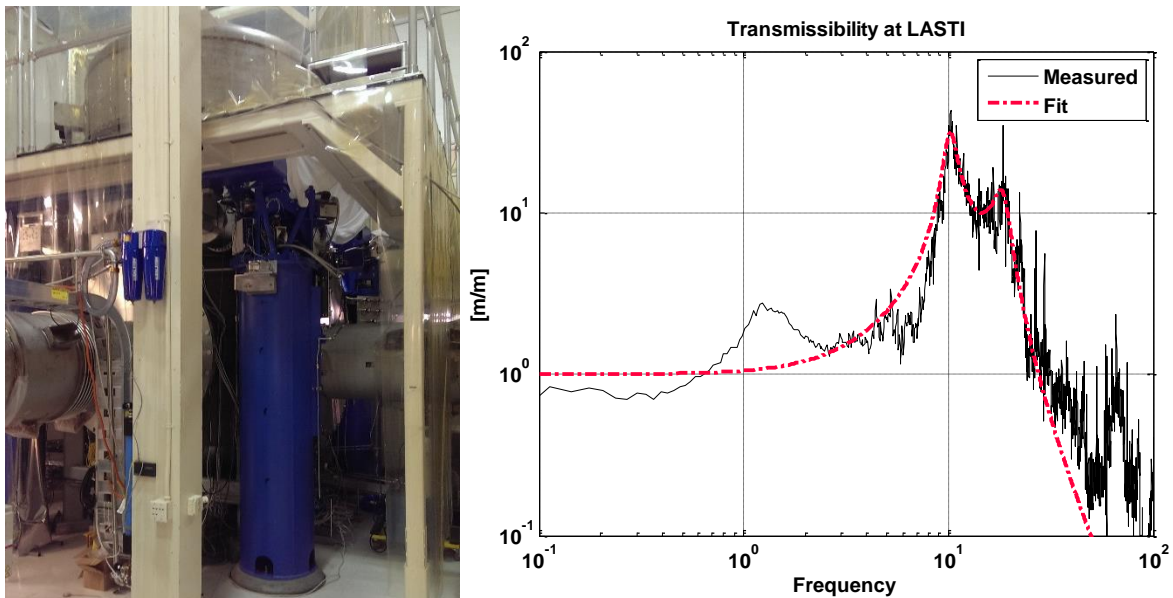

Figure 2: (a) Image of the large chambers and piers at the LIGO tests facilities in MIT, Cambridge MA (also known as LASTI). (b) Plot of the transmissibility between the ground and the top of the piers.

In order to analyze the ground motion at the resonance, inertial sensors have been placed on the floor, around and underneath the chamber. These sensors measure the ground motion in the vertical direction. Figure 3 shows a coherent map of the relative amplitude and phase of the ground motion between these points at the first resonance. The anchorage of the piers is shown by the large circles. Each sensor is represented by a star. Colored interpolation is used to show the amplitude on the left, and the phase on the right. The figure shows that the structure and the ground tilt around a line made by the anchorage of two of the piers.
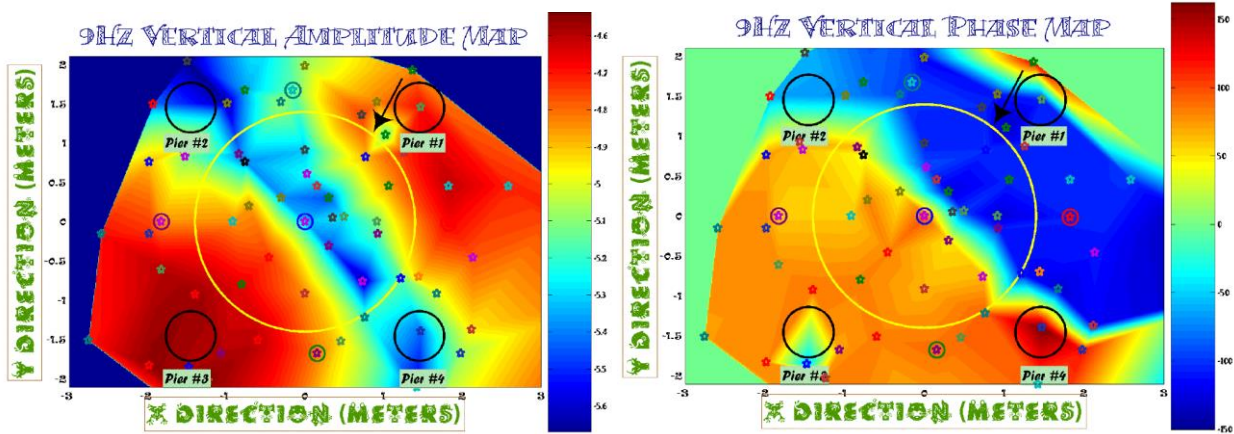

Figure 3: Map of the amplitude and phase of the ground motion in the vertical direction. The structure tilts on the flexible concrete floor [5].

2.2   Advanced LIGO Observatories

Figure 4 and Figure 5 show measurements of transmissibility from the ground to the top of the piers performed at the LIGO Hanford (LHO) and LIGO Livingston (LIGO) observatories respectively. As the observatories are constructed on thicker concrete slab than the LIGO MIT facilities, the motion amplification is not as large, and only one mode is clearly visible. Nevertheless, the motion amplification exceeds a factor of 10. While this excess motion is not critical for the observatories to date, it is important to analyze this vibrational mode and study mitigation options in case it becomes an issue as the LIGO observatories are being commissioned and become more and more sensitive in this frequency range.
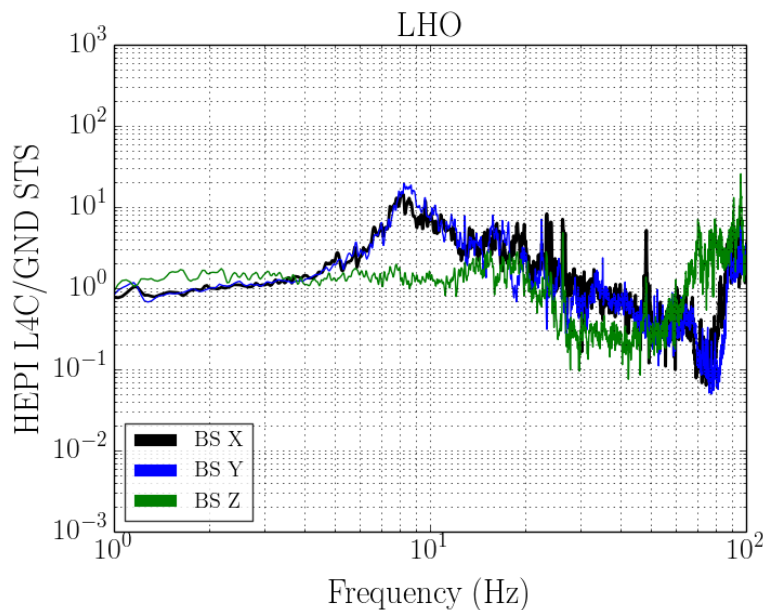

Figure 4: Transmissibility from the ground (GND STS) to the pier top (HEPI L4C) in the horizontal direction (X and Y) and vertical direction (Z) of the Beam Splitter (BS) chamber at the Hanford site.
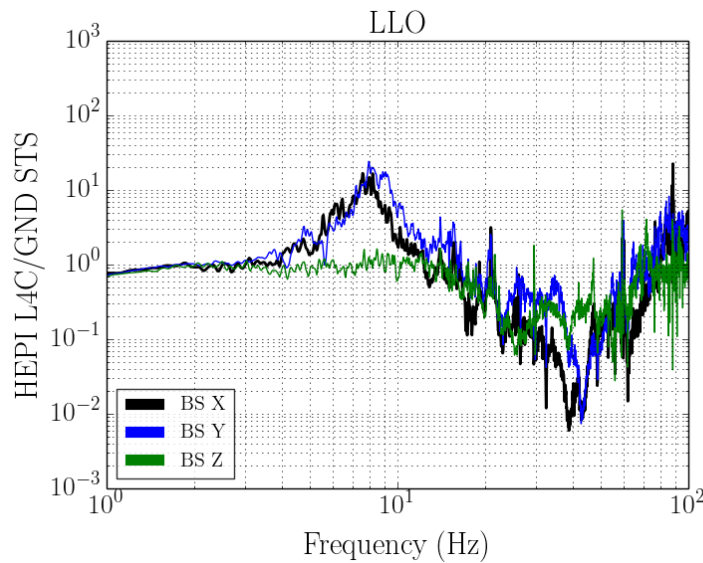
Figure 5: Transmissibility from ground to the pier top in the horizontal direction (X and Y) and vertical direction (Z) at the Livingston site.

3   Modeling

The four large piers discussed in the previous sections support two systems weighing more than 6 tons total. The first system is a hydraulic isolator called HEPI [6]. The second system is a two stage hybrid isolator called BSC-ISI [7]. This section presents a finite element model that has been made to analyze the vibration modes of the entire system. The finite element model of the BSC chamber and the support structure includes (i) the four piers (ii) a simplified model of the HEPI springs assembly (sometimes called housing), (iii) the HEPI support structure (two cross beams and two support tubes), (iv) the BSC chamber, and (v) a model of the concrete floor. The BSC-ISI system is represented by a mass of 1 ton per pier, distributed at the ends of the two support tubes. The chamber is not mechanically connected to the support tubes (i.e. the flexible bellows at the interface, the HEPI structure and the chamber are considered negligible and therefore they are not included in this model). The modeling of the concrete floor is a key component of this model to account for the coupling between the chamber and the piers through the ground.

The piers, the chamber, the cross beams and the support tubes are modeled by shell elements. The mounts of the chamber and the HEPI housing are modeled with solid elements. Rigid links are used to connect parts which are in contact. The boundary conditions impose that all the edges of the ground are constrained in translation (U1=0, U2=0, U3=0). The material used to represent the structure is Steel (E = 200 Gpa , ν = 0.3, ρ = 7600 kg/m^3). The parameters of the ground have been fitted for the model to match with the modal shapes and the corresponding frequencies measured at LIGO MIT test facilities. In the model, the ground has been divided in 2 areas in order to facilitate the fit between the model and experimental results. Figure 6 shows the cross section of the ground in model along the x-direction with the nominal parameters of each area. The central area is made of usual concrete and the peripheral area with a reduced Young's modulus. The piers and the BSC chamber are located on the central area.
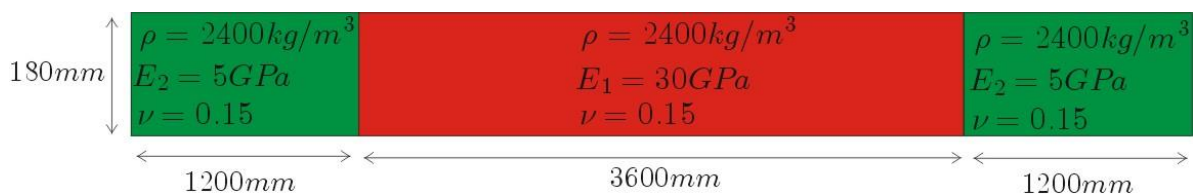

Figure 6: Cross section of the ground in the finite element model along the x-direction. The red section represents the ground below the piers and BSC chamber. The values are the nominal values.

The first six modes are illustrated in Figure 7. Below 20 Hz, the system behaves essentially like a two-mass system, in both horizontal directions (x and z). In this model, the resonance shapes and frequencies are very sensitive to the values of the ground parameters. Figure 8 shows the evolution of the six natural frequencies as a function of three parameters: the ground thickness, the Young modulus of the ground in the surrounding area (peripheral zone) and the Young modulus of the ground in the area below the structure (central zone). For each case, the dotted grey vertical line corresponds to the nominal value of the parameters. In some particular cases, a modification of the mode shapes order has been observed, which has been indicated by encircled numbers. Before presenting some potential techniques for the mitigation of these modes around 9Hz, we briefly remind the reader the well known *Craig-Bampton* sub-structuring method which is used to reduce the number of degree of freedom (d.o.f.) to some retained nodes and modes, and further extract the compliance information used to design the vibration control methods and assess their performances [8].

Mode 1 : $f_1 = 8.92 Hz$

Mode 2 : $f_2 = 9.23 Hz$

Mode 3 : $f_3 = 10.16 Hz$

Mode 4 : $f_4 = 11.15 Hz$

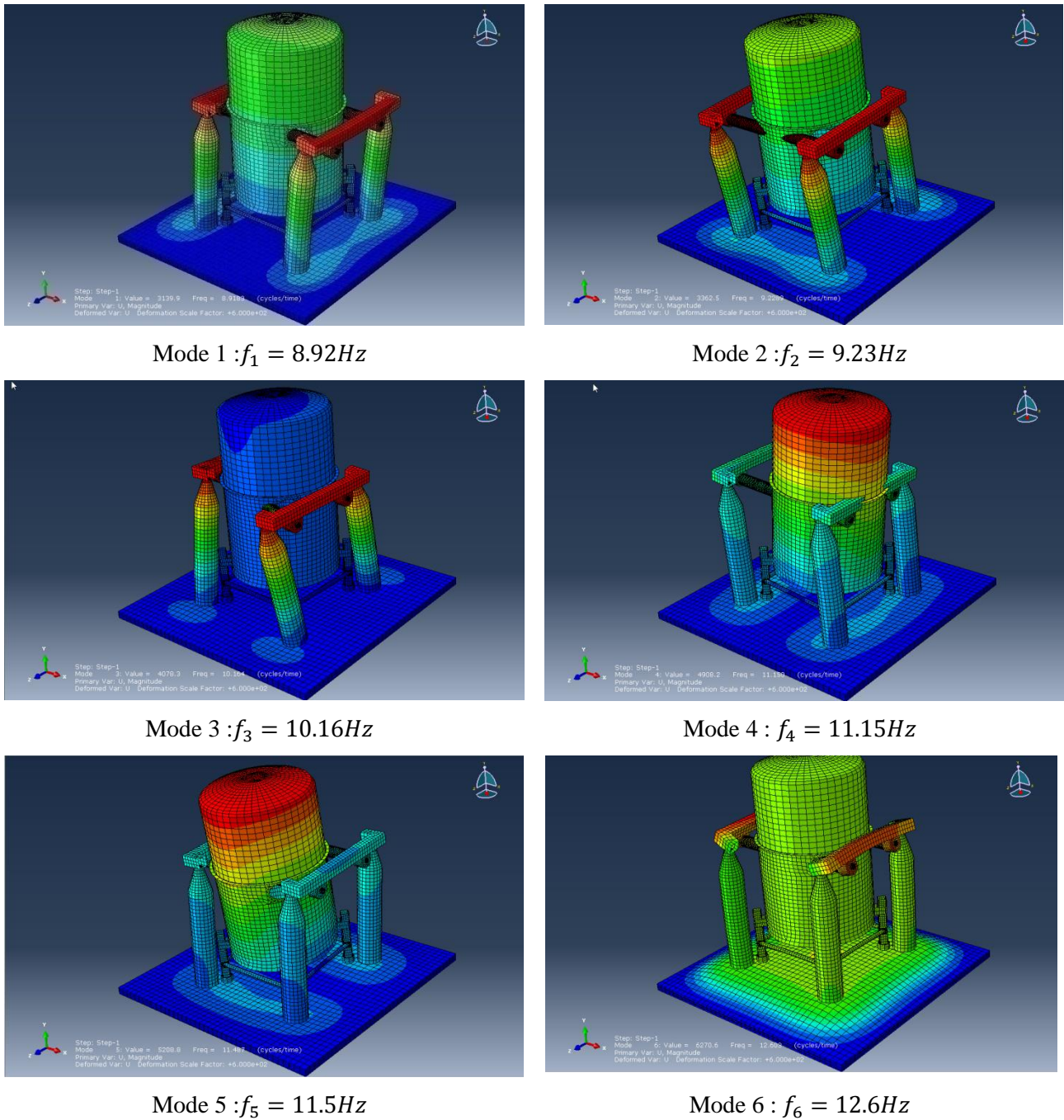Mode 5 : $f_5 = 11.5 Hz$

Mode 6 : $f_6 = 12.6 Hz$

Figure 7: Mode shapes and corresponding frequencies of the first six resonance modes of the structure.
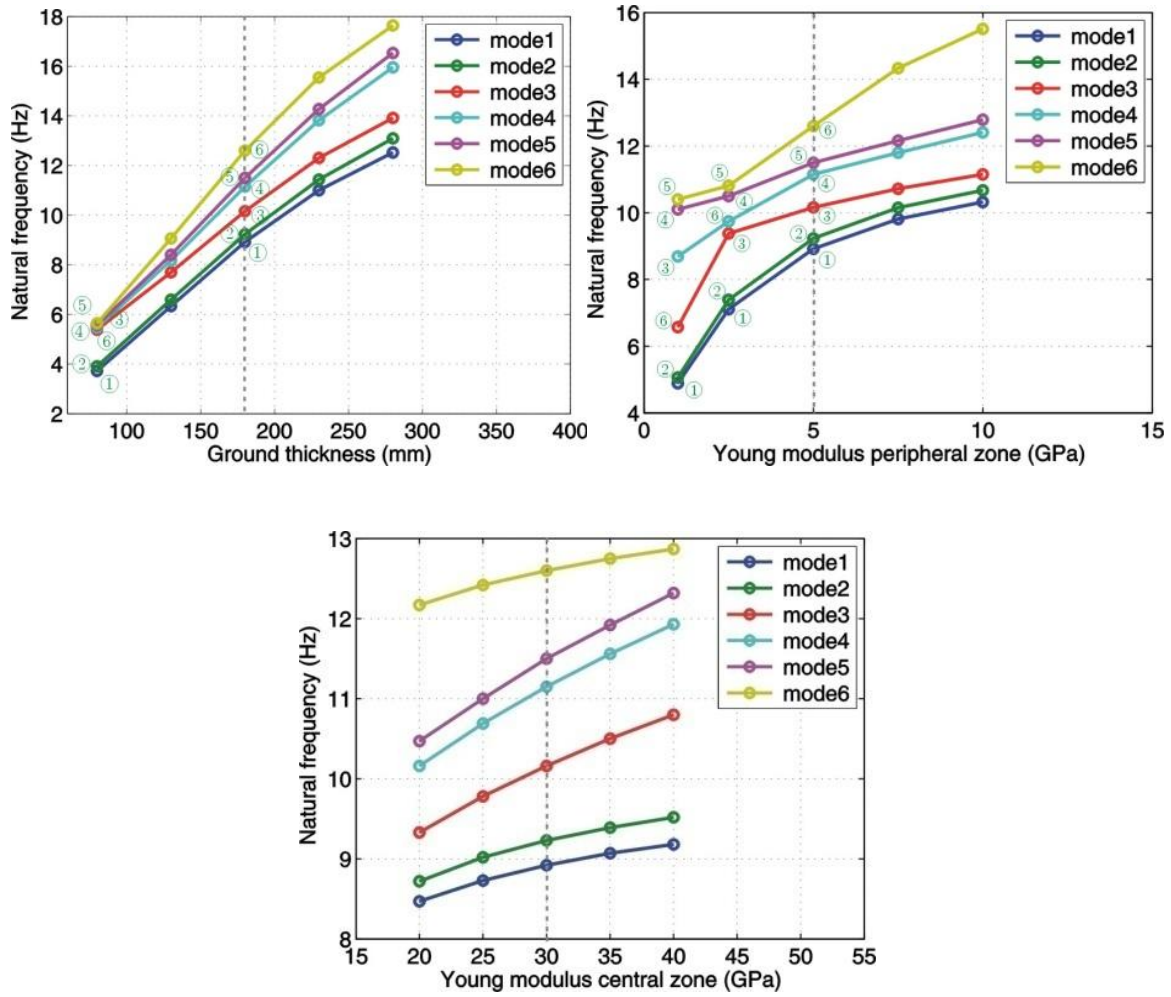
Figure 8: Sensitivity of the first 6 modes natural frequencies with the ground thickness, the Young modulus of the ground in the surrounding area (peripheral zone) and the Young modulus of the ground in the area below the structure (central zone).

3.1   Sub-structuring method

The red dots in Figure 9 show the position of the nodes retained for the computation of the compliances. Those compliance curves are the transfer functions of a state space model build from the reduced mass matrix and the reduced stiffness matrix extracted from a super element generated by the *Craig-Bampton reduction* of the finite element model. The dynamic equations of the finite element model are

$$\begin{pmatrix} M_{11} & M_{12} \\ M_{21} & M_{22} \end{pmatrix} \begin{pmatrix} \ddot{x}_1 \\ \ddot{x}_2 \end{pmatrix} + \begin{pmatrix} K_{11} & K_{12} \\ K_{21} & K_{22} \end{pmatrix} \begin{pmatrix} x_1 \\ x_2 \end{pmatrix} = \begin{pmatrix} f_1 \\ 0 \end{pmatrix} \tag{1}$$

where the d.o.f. have been partitioned into the retained d.o.f. x_1 and the condensed d.o.f. x_2. The retained d.o.f. include all the d.o.f. with a specific interest in the problem: those which are located in potential locations of sensors and actuators to actively control the system. The condensed d.o.f. include all the other d.o.f. which have no particular interest in the control problem. The *Craig-Bampton reduction* is conducted in two steps. First, a *Guyan reduction* is performed [9]. For the Guyan reduction it is considered that the condensed d.o.f. respond statically (i.e. inertial terms are neglected in the second part of Equ.(1)), which leads to the static relationship
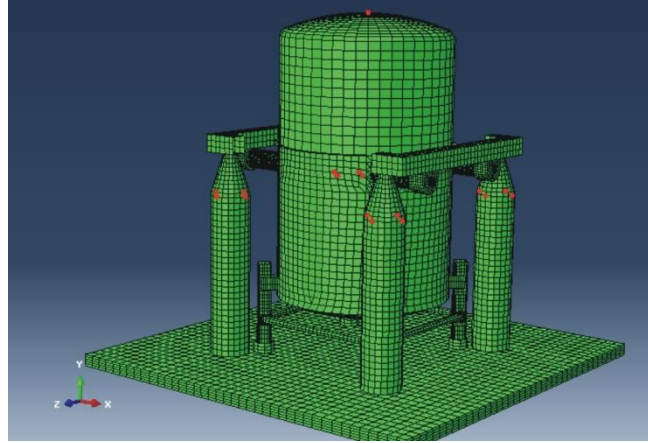
$$x_2 = -K_{22}^{-1}K_{21}x_1 \tag{2}$$

Figure 9: Isoparametric view of the structure. The nodes retained for the calculation of the compliances are shown by the red dots.

In a second step, we calculate the flexible modes by blocking the retained d.o.f., i.e. (1) becomes

$$M_{22}\ddot{x}_2 + K_{22}x_2 = 0 \tag{3}$$

This step allows building an accurate representation of the system if dynamic modes within the super element are important. Let us assume that the eigen modes constitute the columns of a matrix Φ_2, and that they are normalized according to $\Phi_2^T M_2 \Phi_2 = I$. By performing the change of coordinates $x_2 = \Phi_2 z$ where z is the vector of the modal amplitudes we can write

$$x = \begin{pmatrix} x_1 \\ x_2 \end{pmatrix} = \begin{pmatrix} I & 0 \\ -K_{22}^{-1}K_{21} & \Phi_2 \end{pmatrix}\begin{pmatrix} x_1 \\ z \end{pmatrix} = L\begin{pmatrix} x_1 \\ z \end{pmatrix} \tag{4}$$

where L is a transformation matrix. The reduced mass and stiffness matrices $\widehat{M}$ and $\widehat{K}$ are obtained by substituting the above transformation into the kinetic and strain energy, which leads to the dynamics equation

$$\begin{pmatrix} \widehat{M}_{11} & \widehat{M}_{12} \\ \widehat{M}_{12} & I \end{pmatrix}\begin{pmatrix} \ddot{x}_1 \\ \ddot{z} \end{pmatrix} + \begin{pmatrix} \widehat{K}_{11} & 0 \\ 0 & \Omega^2 \end{pmatrix}\begin{pmatrix} x_1 \\ z \end{pmatrix} = \begin{pmatrix} f_1 \\ 0 \end{pmatrix} \tag{5}$$

In this equation, the stiffness matrix is a block diagonal with $\widehat{K}_{11} = K_{11} - K_{12}K_{22}^{-1}K_{21}$ and $\Omega^2 = \Phi_2^T K_{22}\Phi_2$ being a diagonal matrix with entries equal to the square of the natural frequencies of the fixed boundary modes. In order to get an appropriate representation of the system in the requested frequency band, one can increase the number of constrained modes (i.e. increase the size of z) in the reduced model.

For this first finite element model we created a super element by including 25 constrained modes. We used the same number of constrained modes for the simplified beam based model which will be presented below.The transfer functions are then generated from a state space model of the dynamics of the system. This state space representation is expressed in the modal coordinates.

4   Mitigation and recommendation for the future observatories

4.1   Stiffening Investigation at the LIGO MIT tests facilities

Both passive and active approaches have been studied at the LIGO MIT tests facilities in order to stiffen the chambers and pier modes. Passive techniques using struts between the chamber and the facilities structure were unsuccessful. Larger, stiffer struts and more strategic clamping points would have been necessary, but were unpractical.

Active control tests, however, provided promising results. For that, a position sensor was used to sense the relative motion between the chamber and the support structure. A shaker was used to apply a force between its reaction mass and the chamber. A feedback control loop was used between the sensor and the actuator. Inertial sensors were used as motion witness. Figure 10 (a) shows the equipment. Figure 10 (b) shows the plant response, the controller, and the open loop transfer function. The lower unity gain frequency is around 12 Hz. The upper unity gain frequency is around 35 Hz. Figure 10 (c) compares the non-controlled and controlled response. It shows significant stiffening effect in the bandwidth. While, further work would be required to tune the controllers to lower frequencies, this quick test demonstrates that such an approach is an option to reduce the equipment vibrations.
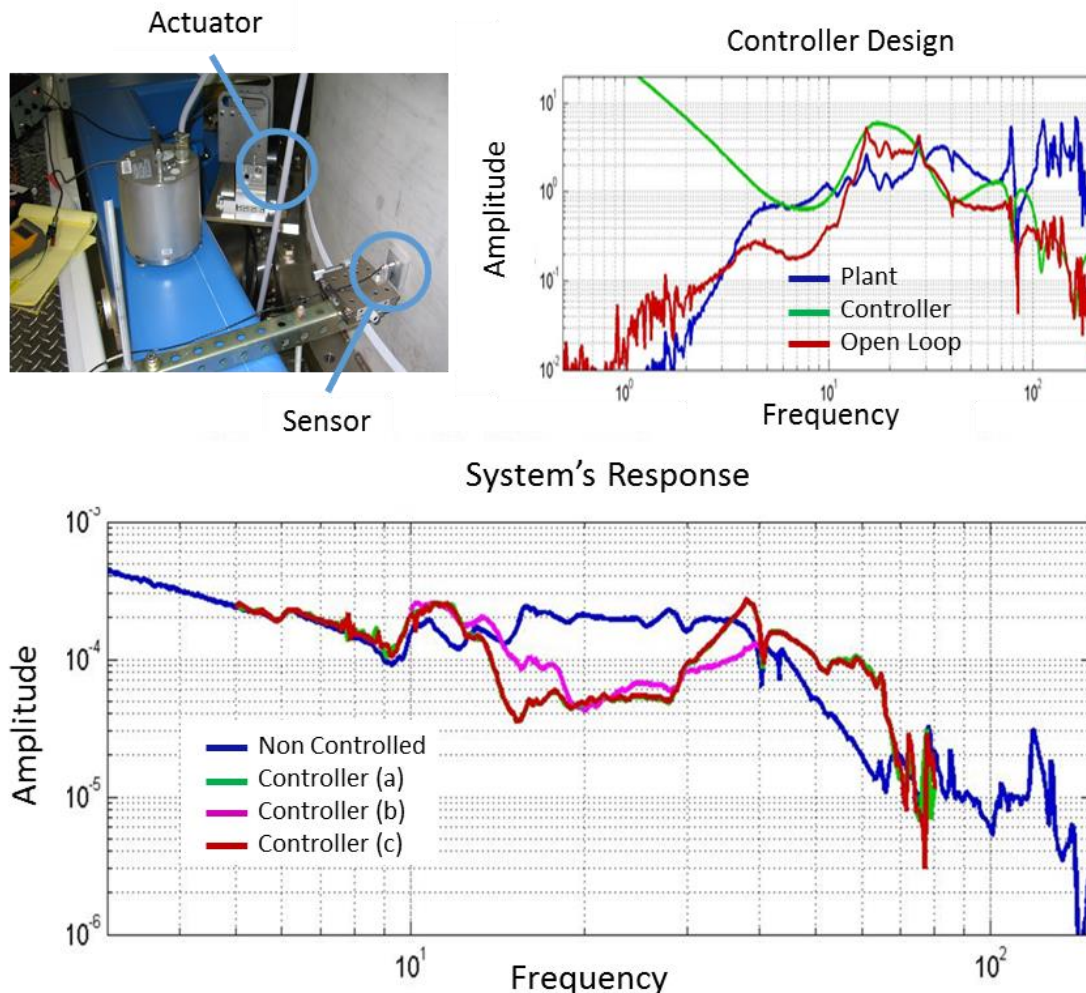

Figure 10: Active control test to inertially stiffen the equipment. Figure a) shows the equipment, b) shows the plant response, the controller, and the open loop transfer function, and c) compares the non-controlled and controlled response.

4.2   Other Control options

Three control options have been implemented on the simplified beam based model to mitigate the pier response around 10 Hz: (1) Mounting a Dynamic Vibration Absorber (DVA) [10] on BSC chamber top or on the pier top, (2) mounting an Active Mass Damper (AMD) [11] on chamber top or on pier top and (3) connecting the piers to the ground with eight active tie rods (two for each pier) [12]. These configurations are described in the following sections, along with examples of pier motion mitigation.

4.2.1   Mounting a dynamic vibration absorber

A DVA is a single d.o.f. oscillator appended on one d.o.f. of the structure, whose parameters (mass, stiffness, damping ratio) are chosen to tune the DVA on a specific mode. For these simulations, we have chosen to append a DVA of 20 kg on the BSC chamber top (the stiffness and damping are calculated according to the so-called *equal peak method* [13]). Figures 11 and 12 show the effect of the DVA on the compliance of one pier, when the DVA is mounted on the chamber top and on the pier top. For both cases, the DVA is always tuned on the first mode of the direction of the compliance. For both directions, the DVA reduces not only the motion of the chamber (not shown), but also slightly the motion of the piers through the flexibility of the ground.
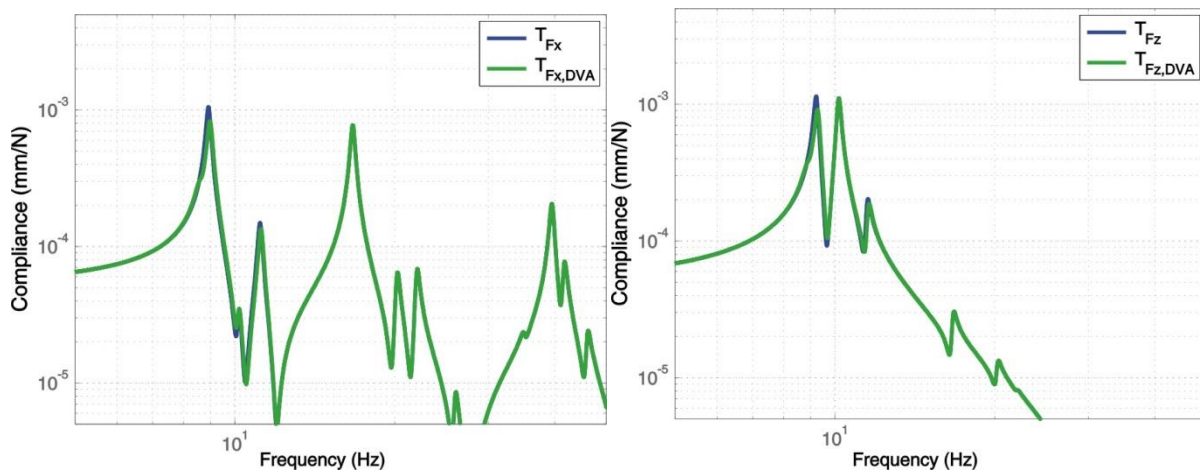

Figure 11: Pier top compliance in direction x (left) and z (right) without (blue) and with (green) a DVA mounted on the chamber top.
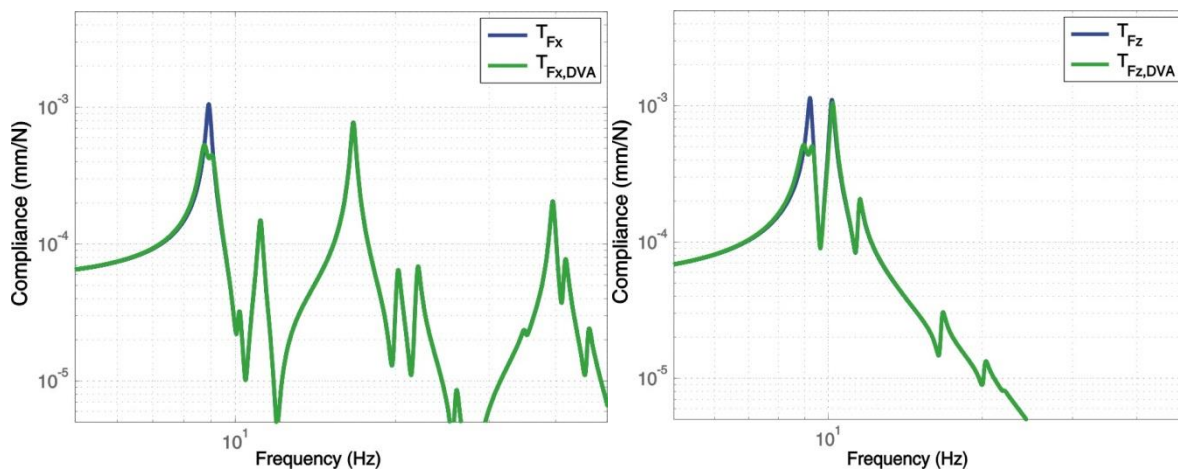

Figure 12: Pier top compliance in direction x (left) and z (right) without (blue) and with (green) a DVA mounted on the pier top.

4.2.2 Active mass damper

An AMD is an inertial actuator, mounted at one specific point on a structure, and driven by the structure velocity at the fixation point. Mathematically, the control force generated is

$$f_i = gH(s)x_i \qquad (6)$$

where g is the gain, the controller $H(s) = s$, and x_i is the d.o.f along which the AMD is working.

Typically, the mass m_a, stiffness k_a and damping ratio c_a of the AMD are chosen in such a way that its resonance frequency ω_a is far below the first resonance frequency of the structure ω_1 (i.e. $\omega_a \ll \omega_1$). We have chosen the following values: $m_a = 20$ kg; $k_a = 3.1583$ N/mm; $c_a = 0.1005$ Ns/mm.

In this section, one AMD is attached to the top of the BSC chamber alternatively along the x-direction and the z-direction. Again, Figure 13 shows the pier top compliance in direction x (left) and z (right) without (blue) and with (green) an AMD mounted on the chamber top. For both directions, the AMD can control the mode at 9Hz to some extent, thanks to the flexibility of the ground.
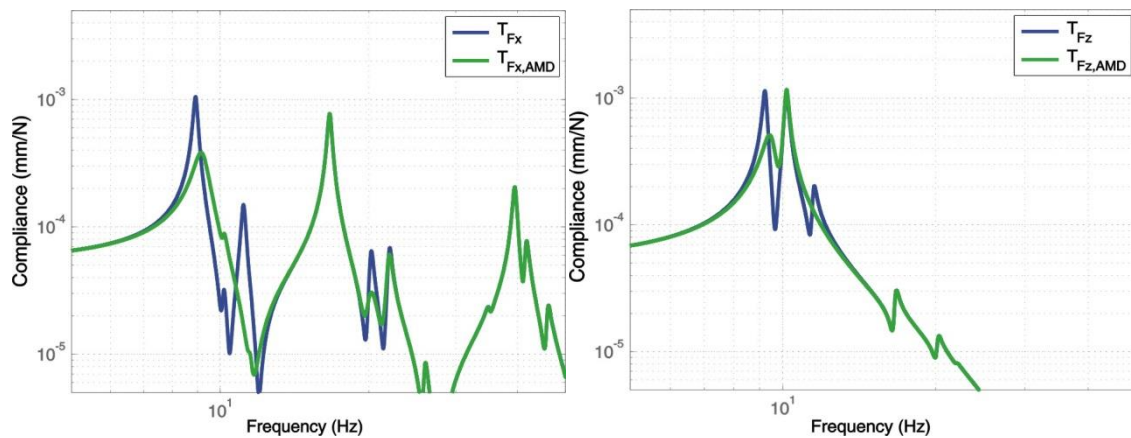

Figure 13: Pier top compliance in direction x (left) and z (right) without (blue) and with (green) anAMD mounted on the chamber top.

Figure 14 shows the pier top compliance in direction x (left) and z (right) without (blue) and with (green) an AMD mounted on the pier top. Compared to the previous case, the efficiency is much better because the AMD acts directly on the pier.
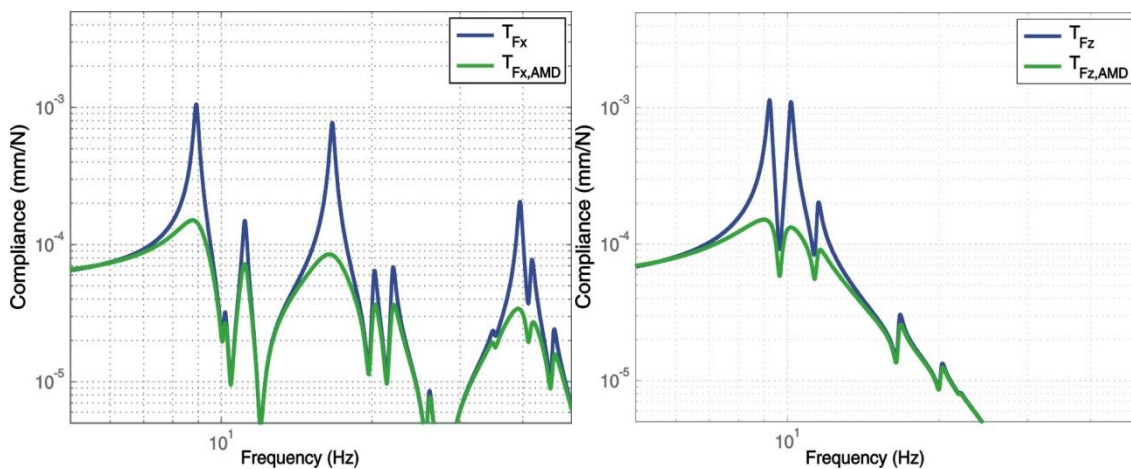

Figure 14: Pier top compliance in direction x (left) and z (right) without (blue) and with (green) an AMD mounted on the pier top.

4.2.3   Active tie rods

Another technique consists of controlling the structural vibrations with a set of active tie rods. In order to have some control authority along the x-direction and the z-direction and also limit the dimensions of the cables, each pier is connected to the ground by 2 tie rods, as shown in Figure 15 (i.e. one in the x-direction and one in the z-direction). The inclination of the cables is α=60° so that the distance between the ground anchorage points and the pier is approximately 1.4m. The chosen stiffness value for each cable is k_c=8.88e4 N/mm. Figure 15 shows the layout of the system.

1. Piezoelectric actuator
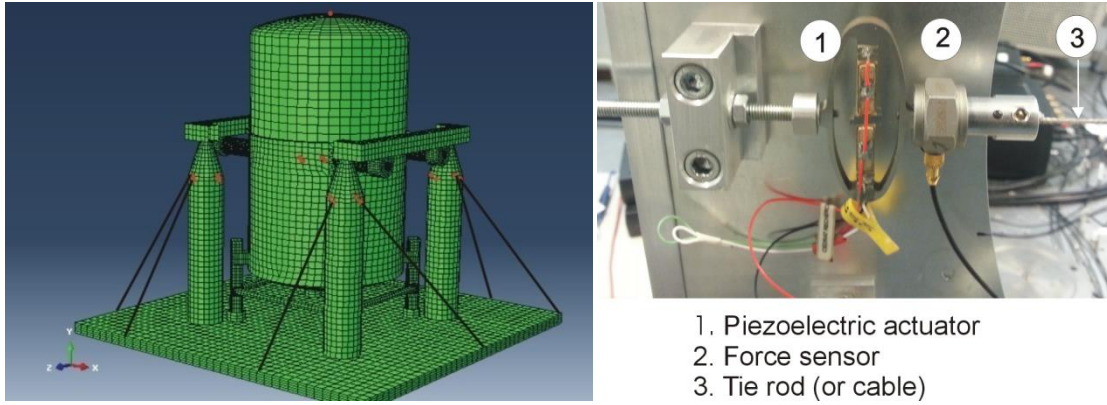2. Force sensor
3. Tie rod (or cable)

Figure 15: Left: Isoparametric view of the structure with 8 controlled cables; Right: picture of an active tendon [14].

The dynamic equation of the system with the rod is :

$$\mathbf{M}s^2\boldsymbol{x} + \mathbf{C}s\boldsymbol{x} + \mathbf{K}\boldsymbol{x} = -\mathbf{B}\mathbf{T} + \mathbf{F} \tag{7}$$

where **M** is the mass matrix, **C** is the damping matrix, **K** is the stiffness matrix, **x** is the vector of structural d.o.f., **F** is the vector of disturbing forces **T** is the vector of the tensions in the cables, and **B** is the influence matrix projecting the tension forces in the structural d.o.f. of the system. The tension T_i in the cable i results from the extension q_i of the cable i such as

$$T_i = k_c q_i \tag{8}$$

and the extensions are also connected to the d.o.f. of the structure by the influence matrix

$$\boldsymbol{q} = \boldsymbol{B^T}\boldsymbol{x} \tag{9}$$

Consider that each cable is connected to the ground through an active tendon, consisting of a force sensor in series with a piezoelectric actuator (See image in Figure 15). The force $F_{a,i}$ measured by the sensor i results from the tension T_i minus the force coming from the elongation δ_i of the displacement actuator, such as

$$F_{a,i} = k_c(q_i - \delta_i) \tag{10}$$

Each tendon is controlled with decentralized Single Input Single Output (SISO) controllers, i.e., that each actuator is controlled using the signal from the force sensor of the same tendon. Mathematically,

$$\delta_i = H_c(s)T_i/k_c \tag{11}$$

where $H_c(s)$ is the control filter. To damp the structure, we integrate the force signal, in order to have a control force proportional to the velocity [12], i.e.

$$H_c(s) = g\frac{1}{s} \tag{12}$$

where g is the gain. In the state space model of the structure, the outputs are the displacements of the top of the piers expressed in the structural coordinate system. The inputs are also expressed in the structural coordinate system. For this reason it is necessary to express the vector of the measured forces $\boldsymbol{F_a}$ in terms of the outputs. The vector of control forces $\boldsymbol{f}$ is expressed as

$$\boldsymbol{f} = k_c\boldsymbol{\delta} = H_c(s)\big(\boldsymbol{B^T x} - \boldsymbol{\delta}\big) \tag{13}$$

which leads to

$$\boldsymbol{\delta} = \frac{H_c(s)}{1+H_c(s)}\boldsymbol{B^T x} \tag{14}$$

The measured forces $\boldsymbol{F_a}$ are then expressed as

$$\boldsymbol{F_a} = k_c\big(\boldsymbol{B^T x} - \boldsymbol{\delta}\big) = \frac{k_c}{1+H_c(s)}\boldsymbol{B^T x} \tag{15}$$

The cable stiffness is given by

$$k_c = \frac{E\pi D^2}{4L} \tag{16}$$

where E is the Young modulus of the material of the cables, D is the section diameter and L is the length of the cables. The simulations have been computed with the following numerical values: $k_c = 8.88e7$ N/m; $E = 200$ GPa; $L = 2846$ mm; $D = 40.7$ mm.

Figure 16 shows the pier top compliance in direction x (left) and z (right) without tendons (blue) with passive tendons (red), with active tendons (green).
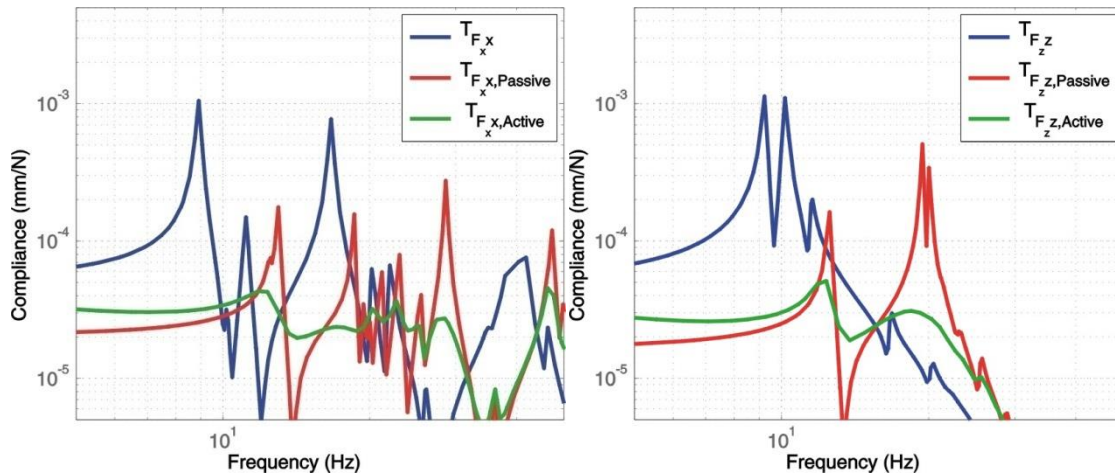
Figure 16: Pier top compliance in direction x (left) and z (right) without tendons (blue) with passive tendons (red), with active tendons (green).

4.3   Recommendations for future observatories

Because of the complexity of the BSC-ISI/soil system, it is not straightforward to have a clear view of the root cause of the amplifications around 9 Hz. In order to understand the behavior of the system in the frequency range between 8 Hz and 20 Hz, numerical simulations and extensive measurement campaign have been conducted at LASTI, and on the sites. Both simulations and measurements have identified the concrete slab's flexibility as a significant contributor to the resonant pier-top dynamics. At this stage, two recommendations may be considered for future instruments in order to increase the damping/rigidity of the concrete basement:

1. Use epoxy concrete in order to increase the loss factor of the concrete basement [15].

2. Make a deeper anchorage of the piers in the ground, and reinforce the metallic armature underneath the chamber.

5   Conclusion

This article discussed the vibration motion of the LIGO observatories large chambers and support structures. The coupling between the chamber and the heavy equipment mounted on the piers happens through the floor's flexibility. It has been demonstrated experientially and by modeling. Tests performed at the LIGO MIT tests facilities showed the viability of active control to reduce the amplitude of vibration. The finite element model condensed by the *Craig & Bampton* method has been used to test several active and passive control techniques to reduce the amplification around 9Hz: dynamic vibration absorbers, active mass dampers, and active tie rods. Their performance has been illustrated using the pier top compliance. Further investigations (e.g. seismic response) are required to make a deeper comparison of these techniques for this specific application. The paper concludes with recommendations to reduce the amplification of the seismic motion induced by the floor flexibility in future instruments.

Acknowledgements

References

[1]   M. MacDonald and V. Badescu, *The International Handbook of Space Technology*, Springer (2014).

[2]   Tshilumba D., Oriunno M., Markiewicz T., and Collette C., *Budgeting and control of the mechanical noise in the International Linear Collider Final Focus System*, Physical review special topics: Accelerators and beams (2014) 17, 062801.

[3]   Matichard F., Lantz B., Mason K., Mittleman R. *et al.*, *Advanced LIGO Two-Stage Vibration Isolation and Positioning Platform. Part 1: Design and Production Overview*. LIGO Laboratory document number LIGOP1200010 (2014).

[4]   Abbott B.P. *et al., LIGO: the Laser Interferometer Gravitational-Wave Observatory*, Reports on Progress in physics (2009) vol. **72** pp. 076901.

[5]   Mittleman R., *2002-2005 investigation on BSC Piers-Chambers motion and Control*, LIGO document, LIGO-E1400247 (2014).

[6]   Hardham C. T., Allen G. S., DeBra D. B., Hua W., Lantz B. T., Nichol J. G., *Quiet Hydraulic Actuators for the Laser Interferometer Gravitational Wave Observatory (LIGO). Proceedings of ASPE conference on Control of Precision Systems* (2001).

[7]   Matichard, F., *et al. Prototyping, Testing, and Performance of the Two-Stage Seismic Isolation System for Advanced LIGO Gravitational Wave Detectors. Proceedings of ASPE conference on Control of Precision Systems* (2010).

[8]   Craig R., Bampton M., *Coupling of substructures for dynamic analysis*, AIAA Journal (1968) vol. 6(7) pp. 1313-1319.

[9]   Guyan R.J., *Reduction of Stiffness and mass matrices*, AIAA Journal (1965) vol. 3(2) 380.

[10]   Frahm H., *Improved means for damping the vibrations of bodies,* GB190923829A (1909).

[11]   Balas M., *Direct velocity feedback control of large space structures*, Journal of guidance and control (1979) vol. 2(3) 252-253.

[12]   Preumont A., *Vibration control of active structures*, 3rd Edition, Kluwer scientific Publisher (2011).

[13]   Den Hartog J.P., *Mechanical Vibrations,* 4th Edition, McGraw-Hill, New York (1956).

[14]   Collette C., Tshilumba D., Fueyo-Rosa L. and Romanescu I., *Conceptual design and scaled experimental validation of an actively damped carbon tie rods support system for the stabilization of future particle collider superstructures*, Review of Scientific Instruments (2013) vol.84(2), 023302.

[15]   McKeown P.A. and Morgan G.H., *Epoxy granite: a structural material for precision machines*, precision engineering (1979) 1(4) 227-229.